

Laboratoire de Physique des Lasers



et



Université de Toulouse

**SPIN MANIPULATION IN A FERMI DEGENERATE GAS
OF ^{87}Sr : IMPLEMENTATION OF A NEW LASER
SOLUTION IN THE EXPERIMENTAL SETUP**

July 7, 2025

Internship Report

Lily Marquié

Supervised by :

Martin ROBERT DE SAINT VINCENT

Contents

1	Introduction	3
2	The ultracold atoms experiment	4
2.1	Atom of interest : ^{87}Sr	4
2.2	Experimental set up	5
3	Setting up a laser diode for laser cooling	8
3.1	Temperature control	8
3.1.1	Thermistor	9
3.1.2	PID loop	9
3.2	Characteristics of the laser diode	11
3.3	Collimation	12
3.4	Cylindrical telescope	15
3.5	Fibre coupling	16
4	Design of the optical chain	17
4.1	The components of the optical chain	18
5	Conclusion	21

1 Introduction

The study of quantum collective phenomena arising in quantum systems is a very current area of interest for physicists. Recent discoveries like superconductivity, uncovered in 1911 by Heike Kamerlingh Onnes, or superfluidity, observed in 1937 by John F. Allen and Don Misener, show the complexity of such quantum systems, and it is an important goal for physicists to comprehend them. It is one of the ambitions of quantum simulation to study such complex N -particle systems that aren't solvable by classical computers. Quantum simulation simulates those systems by creating analogue, simpler systems governed by the same physical laws, using ultracold quantum gases, trapped ions or other platforms. One of the major models these procedures try to recreate is the Fermi-Hubbard Hamiltonian, which describes fermions interacting in the matter. It is central in the domain of strongly correlated systems in condensed matter.

Experimentally, we can realise an ideal and tunable version of this model by placing interacting fermions in an optical lattice. The Magnetic Quantum Gases (MQG) group at the Laboratory of Laser Physics (LPL), where I am conducting my internship, focuses on ultracold degenerate ^{87}Sr gases [1] [2] because of their properties. This isotope of strontium is the only fermion with a nuclear spin of $I = 9/2$, which gives rise to a large Hamiltonian space for the internal degrees of freedom of each atom. The experiment, explained further during this report, carries on a complex temporal sequence in order to trap and cool the atomic cloud at temperatures reaching around thirty nano Kelvins. Only at those temperatures can the cloud reach the degenerate regime where the physics we want to study happens.

Following the acquisition of the gas of interest, many studies can be done. Indeed, the quantum state reached allows physicists to study quantum collective effects that cannot be observed in other systems. In our team, given the fermionic aspect of our system, we focus on creating quantum states interesting for quantum simulation by manipulating the spin states of the atoms. Our latest focus is the development of a new experimental method to obtain totally correlated quantum states called Dicke states for our cloud. Such a state would have a great interest in quantum technologies like quantum computers or simulators. Moreover, it could also be advantageous in quantum sensors, like atomic clocks, because the theory suggests that it could ameliorate the sensitivity and accuracy of interferometers used in atomic clocks. This new method that the team would like to implement uses the concept of photo-association, which is a two-body loss phenomenon. Because the atoms are fermions, the Pauli principle enters the picture and happens to make this phenomenon spin sensitive, allowing the formation of the states of interest described above [3].

In this report, the discussion will not focus on the work done by the team or the future projects to be implemented mentioned above. Nevertheless, the first section will rapidly describe the experiment in which I work as a team with the PhD students. In the second section will be explained in more depth my side personal project: an optical chain I designed and built during this internship.

2 The ultracold atoms experiment

2.1 Atom of interest : ^{87}Sr

The 87 strontium is one of the only 4 isotopes of strontium that are stable and the only fermionic one. It is also the alkaline-earth atom with the largest nuclear spin, with $I=9/2$, which allows it 10 spin states in its fundamental state. This property is interesting because it creates a large Hilbert space of spin states. Some of the important transitions between its electronic states are represented in Figure 1. They are all used in one or multiple steps of the cooling process:

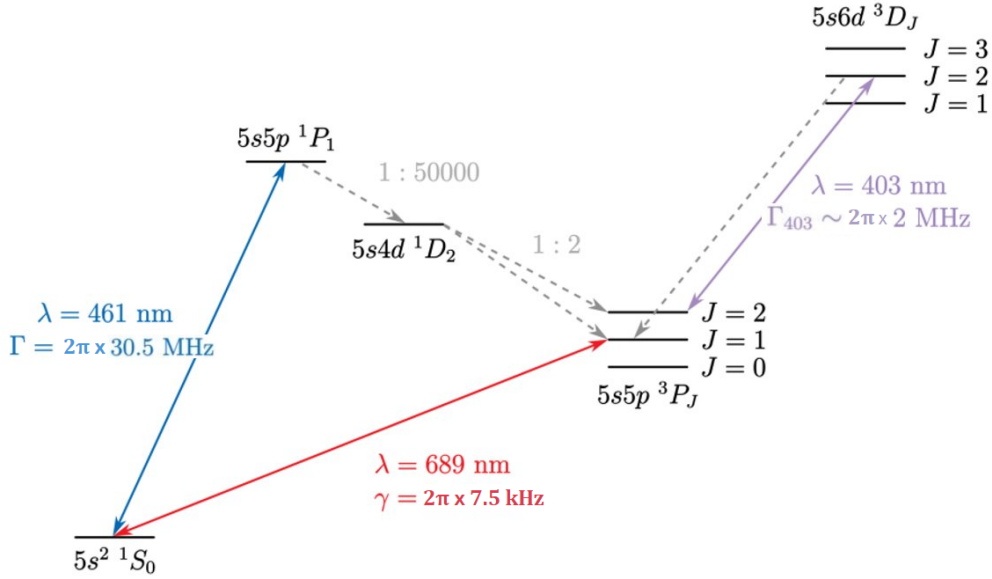


Figure 1: Simplified electronic structure of fermionic ^{87}Sr pointing out the transitions of interest in the experiment. Solid lines represent laser transitions and dotted lines represent additional spontaneous decay paths and their probability.

- The fundamental state 1S_0 : it has 10 spin states from $m_F = -9/2$ to $9/2$. Its small Landé factor creates a weak lifting of degeneracy of its hyperfine states compared to the excited levels. When implementing a magnetic field, the difference of energy between its Zeeman levels can be neglected in comparison with the energy of Zeeman lifting in other states..
- The singlet 1P_1 state: it's the excited state of the 461 nm "blue" laser transition $^1S_0 \longleftrightarrow ^1P_1$ of spectral width $\Gamma = 2\pi \times 30.5 \text{ MHz}$ that we often refer to as the "broad transition" or "blue transition". The singlet state relaxes to the fundamental but also has a spontaneous emission path with a low probability to the metastable states 3P_1 and 3P_2 through the 1D_2 singlet represented in Figure 1 by dotted lines.
- The metastable states 3P_J with $J=0,1$ or 2 :
 - 3P_0 is the excited state of the clock transition of ^{87}Sr .
 - 3P_1 is the excited state of the 689 nm "red" laser transition $^1S_0 \longleftrightarrow ^1P_1$ known as the "red transition" or "narrow transition" line because of its narrow spectral width $\gamma = 2\pi \times 7.5$

kHz. The narrowness of the transition line plus the difference of Landé factors of the excited and fundamental, which gives the metastable state a way larger sensitivity to Zeeman splitting, gives us the ability to resolve every transition from the fundamental to the hyperfine states $F = 7/2, 9/2, 11/2$ of 3P_1 and even each of their Zeeman sublevels m_F .

- 3P_2 is a metastable state of long lifetime used in the experiment to switch between the broad and narrow magneto-optic traps (MOT). Because of its large magnetic dipole moment, the atoms are trapped in the presence of the strong gradient from the magnetic quadrupole of the blue MOT. Half of the spontaneous decay path from 1P_1 ends up in the 3P_1 and half in the metastable 3P_2 . In the former case, the atoms can cycle back to the ground state. In the latter case, the metastable atoms are trapped by the field. By running the MOT for 5 s, the atoms are consistently shelved in the metastable. Then we use the $^3P_2 \longleftrightarrow ^3D_2$ transition at 403 nm to optically pump the atoms and let them decay back to the ground state with a two-photon decay path through 1P_1 . Then the first MOT is switched off and the second one is turned on.
- The triplet state 3D_J with $J=0,1$ or 2 : the 3D_2 state is used for the repumping of the atoms between the two magneto-optic traps.

2.2 Experimental set up

To reach a degenerate Fermi gas, we need to cool the atoms to temperatures approaching absolute zero. Here, the reachable temperatures neighbour the dozens of nano kelvin. For this purpose, we have a complex experimental setup [4][5] explained briefly in the next paragraph.

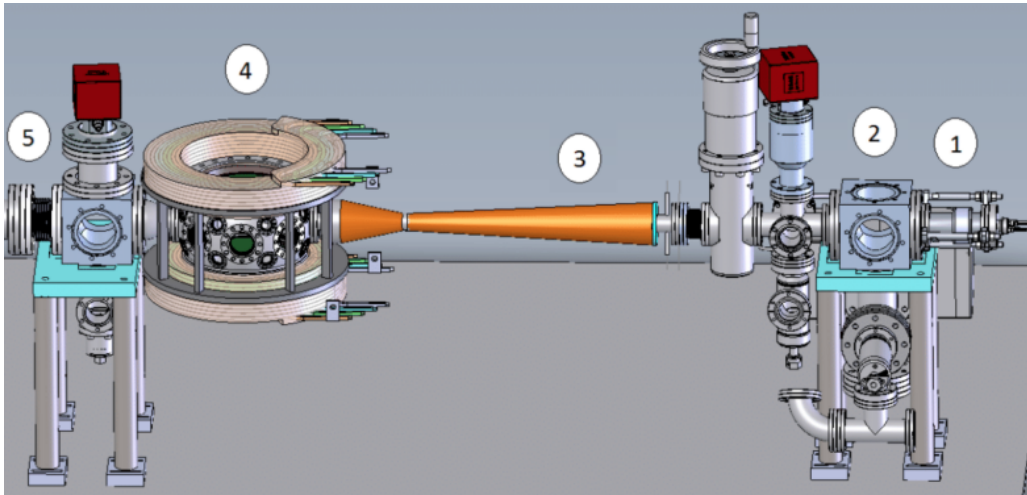


Figure 2: Schematic view of the experimental setup describing the main cooling steps. The heart of the experiment shown here is situated in the centre of the room. The laser beams used in the different stages are sent from multiple optical tables through optical fibres.

1. The oven : We obtain the Sr atoms by heating up to $T = 760$ K solid strontium in the oven. It generates a flux, on leaving the oven, of 6×10^{12} atoms/s with a mean velocity of $v \approx 500 m \cdot s^{-1}$.

2. Transverse cooling (TC) : The atomic flux is collimated out of the oven by transverse 2D optical molasses using the $^1S_0 \longleftrightarrow ^1P_1$ transition. The two orthogonal laser beams, transverse to the atomic beam, are larger in the direction of the atoms' movement to ensure maximum interaction time. They are also red-detuned from the 461 nm transition to interact more with atoms with large transverse momentum thanks to the Doppler effect. As a result, the number of atoms trapped in the later stages can increase by a factor of 2 to 4.

3. Zeeman slower : The broadband MOT's capture speed is 25 m.s^{-1} but atoms after the TC have a mean speed of 430 m.s^{-1} . The Zeeman slower goal is to slow down the flux enough for them to be caught by the broadband MOT. Inside the Zeeman slower, there is a gradient of magnetic field: amplitude decreasing for the first 39 cm and increasing for the next 11 cm. In the initial 39 cm section, atoms are decelerated by a radiative force from a counter-propagating laser tuned to the 461 nm transition. As atoms move and slow down, the Doppler effect causes their resonance frequency to shift. Simultaneously, the Zeeman effect, caused by the varying magnetic field, also shifts the atomic resonance. These two effects are designed to compensate for each other, keeping the effective detuning between the laser and the atomic transition nearly constant over the 39 cm. This allows the atoms to remain in resonance with the laser and be efficiently slowed over the entire length. The second half of the Zeeman slower, where the magnetic field increases over the final 11 cm, serves to shift the atoms out of resonance with the slowing laser. This prevents the atoms from being re-accelerated in the opposite direction once they reach the end of the slower, ensuring they are no longer affected by the radiative force.

Using this procedure, the atoms go from a mean speed of 430 m.s^{-1} at the entrance to coming out with a speed of 25 m.s^{-1} , ideal to enter the broadband MOT.

4. The magneto-optic traps (MOT) : A MOT is constituted of 3 retroreflected lasers, one in each direction of space, of identical circular polarisation and red-detuned from the transition of interest; plus a quadratic magnetic field. It's used to cool but also to increase the density of the atomic gas. The combination of Doppler cooling and Zeeman slowing applies a central return force, slowing and trapping the atoms at the zero-field point.

- The broadband MOT for the $^1S_0 \longleftrightarrow ^1P_1$ is the first one to be activated. This transition is an open loop so we charge the atoms in the 3P_2 with a long lifetime of 10 s. In a characteristic time of 5 s, we can trap approximately 20×10^6 atoms in the metastable state at a temperature $T \approx 1 \text{ mK}$. The minimum temperature reachable in this trap is limited by the Doppler limit of $T_D^{461} = \frac{\hbar\Gamma}{2k_B} \approx 1 \text{ mK}$. Then they are transferred to a second MOT by decreasing the magnetic field gradient.
- The narrow MOT uses the $^1S_0 \longleftrightarrow ^3P_1$ narrow transition. A second laser, called the stir laser, is used to randomise the spin population of the fundamental to prevent strong atom loss [6]. This time the limit for the minimum temperature is given by the recoil energy of one photon: $T_D^{689} = 177 \text{ nK}$ while $T_R^{689} = \frac{\hbar^2 k^2}{2m} = 462 \text{ nK}$. After the last MOT stage, the bulk gas contains 10^7 atoms at $T \approx 10 \mu\text{K}$.

The next step in the cooling process is to transfer the atoms to the optical dipolar trap.

5. The dipolar trap : This last stage is turned on simultaneously with the ending of the red MOT. It is composed of two crossed beams far-off red-detuned at 1070 nm: one elliptical turned on first and called the "reservoir" beam - it exerts a strong containing force on the vertical axis (the axis of its thinnest dimension); and a circular one called the "dimple" beam whose goal is to exert a strong horizontal confinement. Both beams are angled with respect to the vertical and horizontal axes to allow hot atoms to leave the trap because of gravity.

By the end, 25% of the atoms are transferred from the narrow MOT to the dipolar trap. They are cooled to reach degeneracy by forced evaporation. The depth of the potential is slowly lowered, and spontaneous collisions force the hotter atoms to exit the trap. Finally, we reach the degenerate gas regime, otherwise called the Fermi sea.

3 Setting up a laser diode for laser cooling

As mentioned before, the transverse cooling (TC) uses the $^1S_0 \longleftrightarrow ^1P_1$; 461 nm transition line. As of now, the experiment uses a laser diode with an output of 80 mW. However, there are multiple arguments referring to the fact that an upgrade in power for that laser chain would improve the atomic beam collimation performed by the transverse cooling stage and increase the number of atoms trapped later.

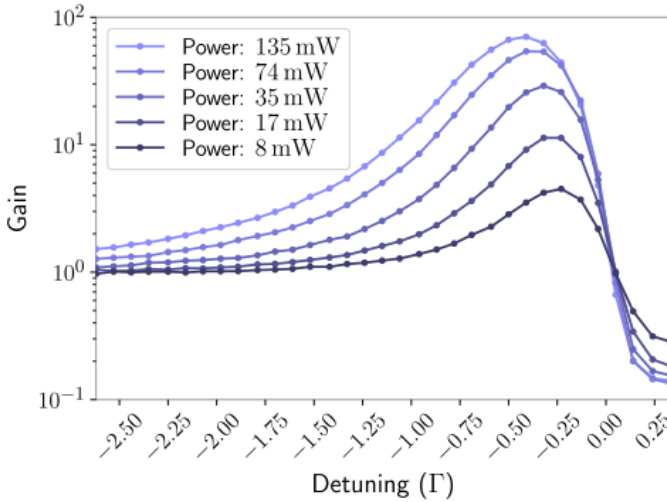


Figure 3: Experimental gain on the MOT loading rate for varying molasses power and detuning measured in Marc Cheneau’s team at Laboratoire Charles Fabry [7] with ^{84}Sr . The gain scale is logarithmic.

One argument is physical: the current laser does not reach the saturating intensity of the atoms. The strontium 87 has a saturating intensity of $40 \text{ mW}/\text{cm}^2$. Our laser interacts with the atoms for approximately 10 cm and is about 1 cm wide in the direction transverse to the atomic beam, which gives a surface of interaction of 10 cm^2 . Hence, the laser would need a power of 400 mW or higher in order to perform its maximal effect on the atoms. The second argument is a graph published in Felix Faisant’s thesis [7] shown in the figure on the left. The maximum gain, i.e. the ratio of atoms in the MOT with and without the TC stage, measured is 70 for a power of 135 mW. We can clearly see an augmentation of the gain with the power of the optical molasses, even if the rate of progression seems to lessen at high powers.

These are the motivations for the work I did during this internship: designing and building a replacement for the blue transverse cooling laser chain. This necessitates multiple steps: characterising the diode, creating a usable laser beam and designing an optical chain to implement on the experiment with its constraints.

3.1 Temperature control

In order to safely power up the laser diode, it’s important to exert control over its functioning temperature. When operating, the diode dissipates heat that could damage it if a cooling system is not implemented. Moreover, our goal is to maximise the gain for a given wavelength, and the laser diode’s frequency varies with the temperature. Hence, the temperature control is primordial. For this, the laser diode’s mount we chose is equipped with a system that can heat or cool (a Peltier), plus a temperature sensor (a thermistor). These tools are managed by an outside temperature controller which, in our case, is also the tool that controls the current of the diode: the ILX Lightwave LDC-3722B.

3.1.1 Thermistor

The mount used, the 234B TEC TO-Can from Arroyo, is equipped with a $10k\Omega$ negative temperature coefficient (NTC) thermistor. A thermistor works by translating temperature into resistance, especially for this one with resistance decreasing as temperature increases, hence the 'negative coefficient'. The equation that links the temperature to the resistance is the following Steinhart-Hart equation :

$$\frac{1}{T} = A + B \times \ln(R) + C \times \ln(R)^3 \quad (1)$$

In the case of this particular NTC, the manual gives us the values of the equation coefficients :

$$A = 1.12924 \times 10^{-3} K^{-1}$$

$$B = 2.34108 \times 10^{-4} K^{-1}$$

$$C = 0.87755 \times 10^{-7} K^{-1}$$

From this equation can be deduced the resistance values necessary to obtain the desired temperatures. The mount has maximum values for working with, which are $65^\circ C$ for the temperature and 4 A for the current injected into it. One needs to be careful, hence the controller is regulated so that the current cannot exceed 4 A. For the most part, we will want to work a bit above room temperature that is set to $21^\circ C \rightarrow R = 12k\Omega$, hence the laser diode will be working at $25^\circ C$ which is equivalent to a resistance of $10 k\Omega$.

3.1.2 PID loop

The laser diode temperature is controlled by a PID (Proportional-Integral-Derivative) loop.

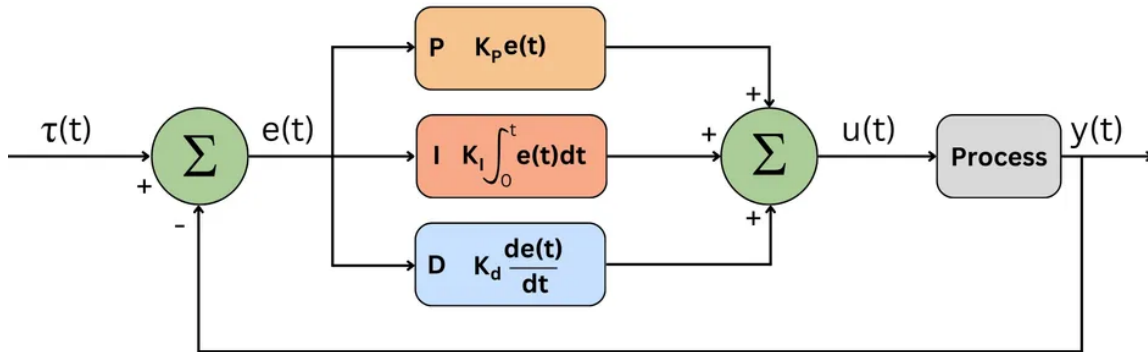


Figure 4: Schematic explanation of the inner functioning of a PID loop. It explains the different components of the loop, their formula and the way they are added/subtracted while the loop functions. Here $\tau(t)$ is the set point value, the desired functioning temperature, and $y(t)$ is the measured process variable, the temperature of the diode. $e(t)$ is the error value continuously calculated by $\tau(t) - y(t)$. The controller attempts to minimise the error by adjustment of the control variable $u(t)$, here the current sent to the Peltier, given by the equation below:

$$u(t) = K_p \times e(t) + K_i \int_0^t e(\tau) d\tau + K_d \frac{de(t)}{dt} \quad (2)$$

We can set the gain of the different parts of the PID loop separately. The goal is to reach the set point value in a finite time with minimum overshoots and oscillations. The 3 gains offer different

advantages and disadvantages.

- **Proportional gain:** depends on the current error.
A high gain increases the speed of response but can create oscillations around the set point value. On the contrary, set a gain too low and the circuit cannot respond to changes at all.
- **Integral gain:** depends upon the accumulation of past errors.
It is effective at reducing the response time and eliminating steady-state errors, but a high gain can produce significant overshoot, oscillations and instability while a gain too low will render the circuit too slow.
- **Derivative gain:** depends on the prediction of future errors.
Its goal is to slow the system to compensate for overshoots by predicting the next step error. Effectively, it enables stronger P/I gains without overshoot, thus faster convergence.

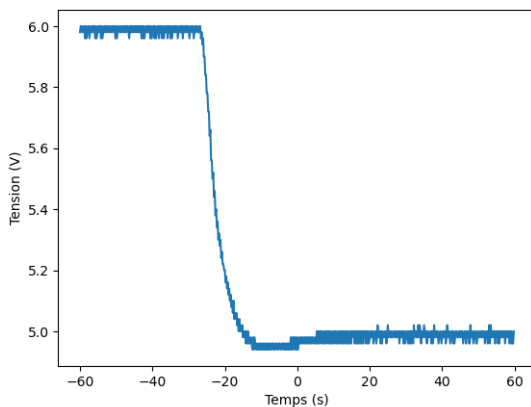


Figure 5: Output voltage of the temperature controller, proportional to temperature, as a function of time

By optimising the parameters of the PID loop, we are able to reach a regime where the set point value is reached in under a minute with only one small overshoot as can be seen in Figure 5. The graph shows voltage delivered by the controller, which is proportional to the temperature, plus the resistance, whose relation to temperature is given by equation (1), is displayed on the device. The resistance starts at $12\text{ k}\Omega$ (room temperature) and reaches $10\text{ k}\Omega$ within 50 s after turning on the temperature controller. There is a small overshoot of 0.2°C that can be seen in the graph. However, it's the best compromise between oscillations and speed that can be reached with this controller.

The next necessary step is to characterise the possible errors linked to this temperature controller. At first glance, there are two issues. First, the controller only allows 3 significant numbers for each constant of the Steinhart-Hart equation A, B and C, and second, the temperature set point value can only be set in $^\circ\text{C}$ and not in terms of the resistance, in Ω . After multiple measurements and calculations, the two kinds of error were recognised and quantified. The rounding of the NTC coefficients creates an offset of 0.03°C between the set point value and the actual value reached in degrees. However, this is a quantified recurrent error, and it can be discharged by simply calculating for ourselves the real value in $^\circ\text{C}$ reached by the temperature control loop. Moreover, the range of error of 0.03°C is too insignificant to affect any characteristic of the diode. For example, since the laser diode is always set to work at 25°C on the controller digital display, we know that the actual value is more about 24.97°C .

The second error, which cannot be modified, is the oscillation of the set value. In the usual case, if the set point value is 25°C so equal to $12\text{ k}\Omega$, there is an oscillation of $2\text{ }\Omega$. This creates an uncertainty

of 0.005°C to 0.01°C which is acceptable for our system because once again it cannot modify the properties of the diode.

3.2 Characteristics of the laser diode

The new high-power solution is the 500 mW Nichia blue laser diode NDB4916. Its characteristics and dimensions can be found in its technical pdf [8]. This laser diode is not encapsulated in an extended cavity, but the lasing phenomenon is happening because the facets of the diode are weakly reflective. However, this does not give any control over the emitted wavelength. The frequency regulation will be ensured with an optical injection-lock described later on. The collimating optics will also have to be chosen and placed afterwards. As written in the pdf, the different values characterising the laser diode, i.e. current threshold, wavelength, etc, can only be given within a large range. Indeed, even when manufactured by the same process, one diode's specifications vary from the next. They are also temperature-dependent. Thus, to possess full knowledge of the laser diode we are using, there was a need to perform measurements to characterise it. This process was also a chance to learn the correct way to make measurements as well as pinpoint and quantify the uncertainties, as needs to be done for every physical measurement.

The first step was to determine the lasing threshold, which is the lowest current at which the laser's output is dominated by stimulated emission rather than spontaneous emission.

For the assessment of the uncertainties on the current and power values collected, the primary uncertainty is given by the tools. The power meter has a given precision that characterises its measurements, and the current generator has an uncertainty on the difference between the current value displayed and the actual current delivered. In our case, both displays have a precision of 3 significant digits.

The second element that can cause uncertainties is the environment. By switching the room's light on and off, we verified that it had no influence on the power measured. The position of the photodiode employed to measure the power has also been looked at. If one is careful enough to place the photodiode each time where the signal is the most intense, then it has no influence either, i.e. the values collected do not vary. The laser diode operating temperature has an influence, but it is controlled as explained before by a PID loop. Lastly, the exact wavelength of the light emitted can impact the measurements. As a matter of fact, the photodiode electronics calibrated to give the "power" information rely on information of the wavelength entered by the user, and the wavelength is not known as it can vary (with regards to the temperature and current for example). However, by measuring the wavelength using a wavemeter while the temperature control loop was in place, we showed that the wavelength fluctuations amount to uncertainties insignificant by comparison to the tool's one (significant digits of display). However, these are two different types of uncertainty: a precision one and an accuracy one, so both need to be taken into consideration. Nevertheless, we can say that the uncertainty given by the fluctuations of the wavelength is not the main source of error.

The graph obtained, shown in Figure 6, is a 2-part curve: a current section with $P=0$ and a current section with $P = aI + b > 0$. By obtaining the linear fit on the second section, the slope and lasing threshold can be determined. However, the value derived should have a physical sense; hence, the numerical fit should take into account the uncertainties.

The most common method of fitting the least squares used to fit data does not handle errors on both X and Y values. Therefore, the uncertainties on both values of current and power were simulated by running 1 million Monte Carlo runs of linear regression.

For each run, the experimental points are taken from a normal distribution with a mean value equal to the value measured and a standard deviation equal to the uncertainty. Then, a linear fit is performed and measuring the standard deviation on histograms of values for a and b gives the final uncertainties.

Linear Fit: $P = (1.389 \pm 0.001 \text{ mW/mA}) \times I - (63.857 \pm 0.061 \text{ mW})$

The threshold is calculated using $-b/a$ and its uncertainty using the mathematical relations linking the uncertainties for a division.

Threshold = $45.963 \pm 0.047 \text{ mA}$

Both of these values are in accordance with the ones given by the manufacturer [8].

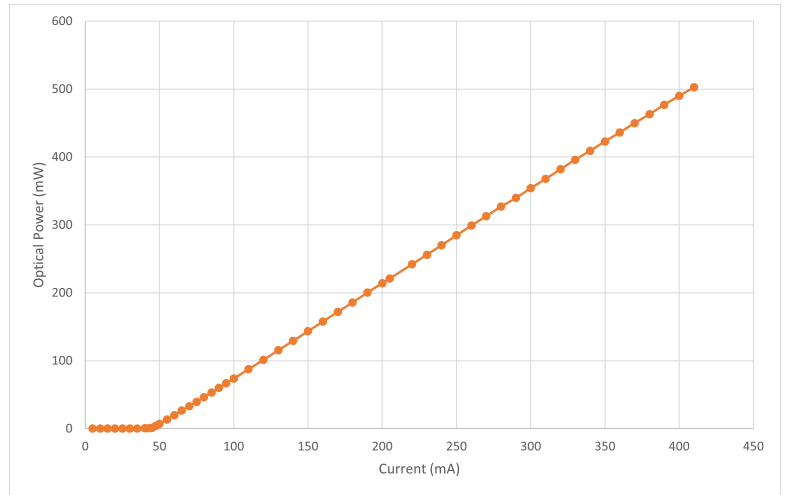


Figure 6: Output optical power in mW depending on the input voltage in mA. The circles are experimental points and the error bars are too small to be visible. We can clearly observe the lasing threshold point and the linear evolution of the output power.

3.3 Collimation

At the output of the mount, the beam needs to be collimated because it is highly divergent. Moreover, the divergence depends on the axis. The total beam divergence of this laser diode is given in the specifications: 24.0° for the vertical axis (also called the rapid axis) and 9.0° for the horizontal one (called the slow axis). The choice of the collimating lens needs to be done carefully by taking into consideration the beam divergence and the desired beam waist at the output. In our case, the goal is to obtain a waist of the order of $500\mu\text{m}$.

By a quick graphical understanding of the situation, one can write the equation linking the parameters: $\tan(\theta) = \frac{\phi}{f}$ with f the focal length, ϕ the beam waist at the lens and θ the beam semi-divergence, hence $\theta_v = 12.0^\circ$ and $\theta_h = 4.5^\circ$.

Lenses only come in a handful of focal distances, so our choice landed on a lens of $f = 3.1\text{mm}$. The calculations give an output of $w_h = 0.24\text{mm} = 240\mu\text{m}$ mm and $w_v = 0.66\text{mm} = 660\mu\text{m}$. When

choosing a lens, one also has to make sure that it will not create aberrations. To check for any issue, we compare the numerical aperture (NA) of the lens given by the manufacturer and of the beam that enters it: $NA_{LENS} = 0.68 > NA_{BEAM} = \sin(12) = 0.21$. This lens can be used for the system without a problem.

After the choice is made, the lens is placed in a cage system attached to the laser diode's mount by four rods and tightened by side screws. The lens can be moved inside the threaded cage. Two parameters have to be carefully calibrated: the centring of the lens on the laser diode's light and the distance between them. Both are rigorous jobs as the output beam is very dependent on the placement because of its short working distance $d=1.8$ mm. The centring is managed by looking at the output using a divergent lens (here $f=-75$ mm), checking the symmetry of the light profile and using the side screws to maximise it. For the distance, the collimation is checked i.e. we want the beam to be approximately the same size for the next few meters available on the breadboard. However, perfect collimation is not a real physical possibility because, due to the diffraction phenomenon, every beam ends up widening.. The realist objective is to form a beam with a Rayleigh range sufficiently long to encapsulate the next few optics on the optical chain. The Rayleigh range is the range after which the dependence of the waist with regard to the distance becomes linear, and in physics, it's comprehended as the range within which the divergence is acceptable. Our centring and collimation were done with precision. However, given the initial divergence of the light, the beam is still elliptical as can be seen in both pictures in 7.

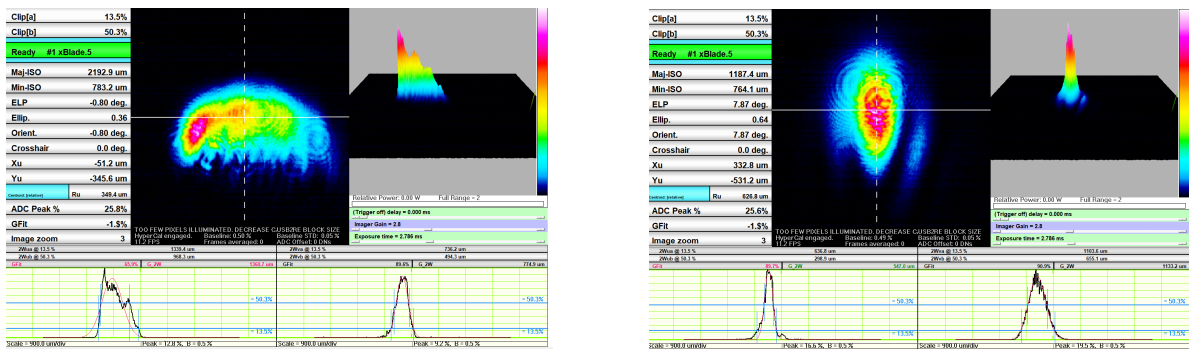


Figure 7: Pictures taken by a camera and fits done on the laser diode beam profile after collimation. The pictures are rotated by 90° compared to reality because of the placement of the camera. The left picture was taken at the focus of the horizontal axis, around 75 cm after the diode. The right one was taken at the focus of the vertical axis, around 1.5 m after the diode.

To characterise thoroughly the beam and its propagation, measurements were made of the beam's size at different distances from the diode. The results gave a linear dependency between waist and distance, which was not what was expected given that a collimation had been done previously and the observations were different (see caption of Figure 7). However, the laser diode has been moved in the few weeks between, thus the situation may be different. The hypothesis is now that the focus must have moved to the rear of the diode. To verify such supposition, we placed a lens of $f = 150\text{mm}$ after the output, and the goal was to observe the propagation of the beam afterwards, and determine the focus' size and position. The values for the same quantities before the lens could then be calculated using the ABCD matrix method.

The mode of the diode is dependent on the current injected for such multimodal diodes so we

wanted to make the measurements at high power. However, the camera has a maximum sensitivity threshold and cannot hold 500 mW. The solution was to place a $\lambda/2$ wave plate, plus a polarising cube to select and send only a small percentage of the light to the camera. The results were then exported and fitted using a Python script. The waist for each position along both axes was determined and plotted with regard to the distance. The results are shown in Figure 8.

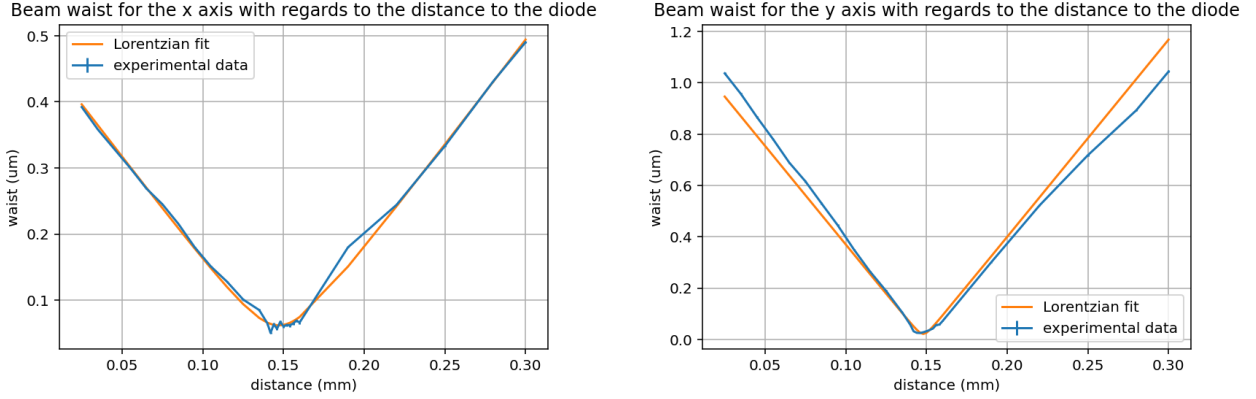


Figure 8: Experimental data plus Lorentzian fits for both vertical (x) and horizontal (y) axes. Fits were done using the numpy function curve fit with the function to fit given below 3. For each point, the uncertainty on the waist determined by numerical calculation is taken into consideration. However, they are too small to be visible on the graph.

The formula for the fit is:

$$w(z) = w_0 \sqrt{1 + \left(\frac{(z - z_0)}{z_R}\right)^2} \quad \text{with } z_R = \frac{\pi \times w_0^2}{M^2 \lambda} \quad (3)$$

with w_0 the focus' size, z_0 the focus' position, $\lambda = 461 \text{ nm}$ and M^2 the beam quality factor. And the results give:

- X axis : $w_0 = 62.00 \pm 2.41 \mu\text{m}$, $z_0 = 147.07 \pm 0.65 \text{ mm}$ and $M^2 = 1.35 \pm 0.05$
- Y axis : $w_0 = 21.48 \pm 4.2 \mu\text{m}$, $z_0 = 148.06 \pm 0.58 \text{ mm}$ and $M^2 = 1.13 \pm 0.22$

The value of the M^2 for both fits is close to 1, which characterises a decent beam, and the focus' size and position were given with uncertainties. The time was too short, but the next step, as mentioned earlier, is to calculate the values before the lens to verify our hypothesis.

We also questioned the future importance of having a round beam and concluded that it will indeed be highly significant. Indeed, the laser will be injected by a master laser, controlled in frequencies, and the coupling between those two beams depends on the similarity of the shape of their profile. Hence, to maximise our coupling efficiency in the next steps, we need to implement a lens system to make the beam round.

3.4 Cylindrical telescope

The telescope uses two cylindrical lenses. Cylindrical lenses are lenses defined by a fixed radius of curvature along one axis. Their form creates a difference in treatment between the two orthogonal axes: the light on one axis will not be modified (neutral axis) while on the other, the light will undergo the modification given by the focal distance of the lens (either convergence or divergence). Thus, by putting a divergent and a convergent cylindrical lens, one can magnify only one axis of the beam.

In our case, we want to magnify the horizontal axis by a factor of two to reach approximately a round beam ($w_h = 240 \times 2 = 480 \mu m$ and $w_v = 660 \mu m$). The ratio between the focal lengths gives the magnification ratio: $\frac{f_2}{|f_1|} = 2$, so the telescope is composed of a cylindrical divergent lens of $f_1 = -50$ mm and a cylindrical convergent lens of $f_2 = 100$ mm. To correctly position both lenses, I first identified their neutral axes by observing the beam after it passed through each lens individually. I looked for the lens angle that magnified the vertical axis, as it was easier to observe due to the beam's larger size. Then, I rotated the lenses by 90° from those angles to align the neutral axis vertically and the active axis horizontally. The only variable left is the space between both lenses. As a matter of fact, we can use this particular distance to correct another negative aspect of our output beam: the astigmatism. A beam is astigmatic when both axes do not converge on the same spot; hence both foci are not at the same place. I proceeded to choose the distance by watching the waist of the beam on both axes and finding the distance that erased the astigmatism of our beam.

Because of the nature of the diode, the beam's mode is not really Gaussian. To characterise the spatial mode, I placed a 200 mm converging lens. By placing the camera and capturing the beam at the focal plane, also called the Fourier plane, we observe the separation of different components of the light. Indeed, in the Fourier plane we observe the Fourier transform of the light. The different components will be spatially dispersed by this transformation, and by capturing the centre part, we can distinguish the centre mode of the light, which will be the one to propagate through the optics and fibres. In our case, we observe the Gaussian mode of Figure 9.

This mode is highly satisfactory, given the deformed profile of the beam before the telescope. The first observation is the acquisition of an stigmatic beam. By sliding the camera along the laser propagation axis and monitoring the size of the spot, we were able to conclude that both directions focus at a identical position. Moreover, the data were retrieved from the camera software DataRay and processed into a python script for a more performing Gaussian fit. The conclusion is that a Gaussian is a near perfect fit for the signal, plus the waists deducted for both axis are similar. We reached a Gaussian round and stigmatic mode; hence all the objectives of the telescope are completed. Still, a slight loss in power is to be expected when concentrating only on the Gaussian mode. The 2D profile contains most of the optical power inside the Gaussian fits, however a little percentage-not even 5% by eye- is contained inside the small pics on the sides that can be seen mostly on the vertical fit of Figure 9 (bottom left of the picture).

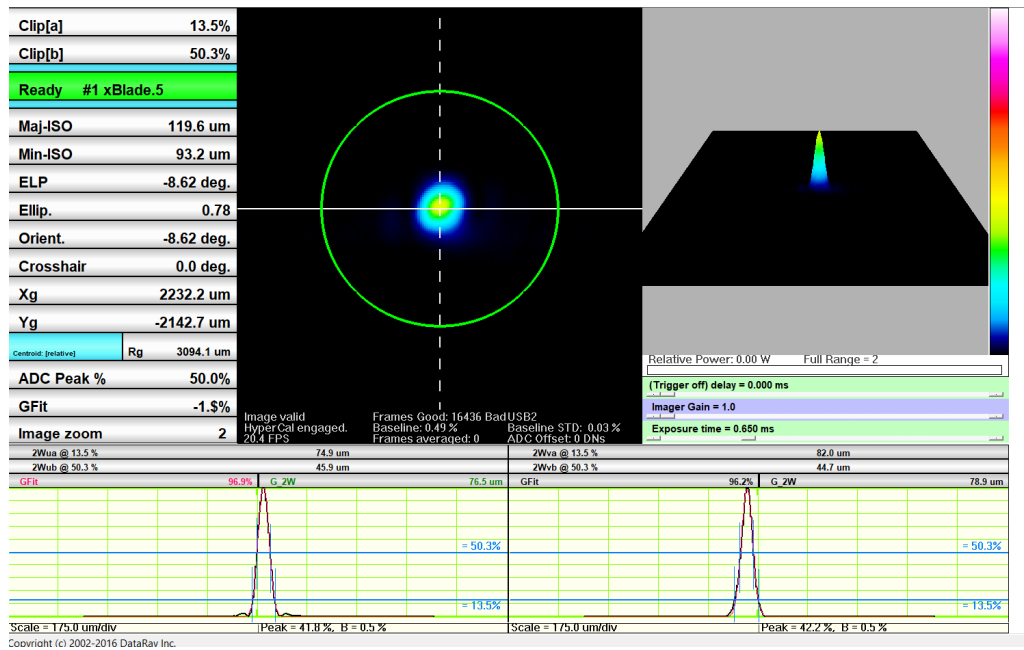


Figure 9: Picture and gaussian fits performed by the camera on the beam after the telescope and a 200 mm converging lens. Above are the picture taken by the camera and the 3D modelisation with the intensity. Below are the fits for the x and y axis and the values of the waists at 13.5% and 50% deducted from them. However, these fits are poor quality because they are made from a cut of the image where the white line is placed by the user and not from integrated values.

3.5 Fibre coupling

Another big question about the design of the setup revolved around the use of fibres because of the constraints. Since the space available to place the setup close to the vacuum chamber was cramped, we thought about injecting the beam into optical fibres to be able to place the optical chain elsewhere. However, the entire point of changing the laser solution is to increase the power sent inside the vacuum chamber and injecting a laser inside a single mode fibre can mean big losses of power.

In order to make a choice, we needed to know the coupling efficiency of the laser beam inside a single mode fibre to assess the losses and decide if the practicality is worth it. The coupling of a fibre is a rigorous task that requires to follow a detailed guideline.

Here are the steps I followed in order to obtain maximum efficiency :

- Choose the fibre and collimating lens. The fibre needs to have a cutoff wavelength smaller than the laser beam wavelength but still close to it. Then, the numerical aperture (NA) of the fibre, the focal length of the collimating lens and the waist of our beam are linked by the formula : $w = 0.82NA \times f$. Knowing the dimensions of our beam $w \approx 500\mu m$, the optimal parameters for both the lens and fibre can be determined within the choices available : for the lens $f = 4.5$ mm and the P3-405BPM-FC-10 fibre with $NA = 0.12$.
- Align every optic. To avoid unnecessary struggles in the future, it is important to make sure that every optic is aligned well before starting. That means verifying the beam is following the holes in the breadboard and that it runs horizontally, that it hits the mirror in the centre and at 45° . Also that every component is mounted at a similar height. Both mounts for the mirror

and collimating lens should have degrees of freedom given by knobs for both axis otherwise the adjustments cannot be done correctly.

- Roughly adjust the position of the collimating lens on the optical axis. In prevision of future issue, it is easier to adjust the distance between the lens and the fibre entrance at the start. I used the handheld fibre coupled Thorlabs HLS635 to send some light from the other side. Then I moved the lens and adjusted the distance in order to collimate the output of the fibre.
- Center the beam on the collimator. Without putting on the fibre yet, we need to centre the beam by eye to make it easier to have a signal when inserting the fibre. Using the mirror knobs, we move the beam so that it passes through the mount and is visible after, and using the other knobs we tilt the mount to focus the light at the centre of the its shadow. The steps are repeated until it converges.
- Introduce the fibre. Using a power meter, we can measure if there is any light at the output. In my first try, I couldn't see any signal so I pulled out slightly the fibre. Then I maximised the power by touching the 4 knobs of both mounts. By optimizing the power while screwing gradually back the fibre, we reached the closed position with a signal of a few μW .
- Find the maximum output power. First by touching individually the knobs from the mirror mount and collimator mount, I maximized the output power. If the job is done correctly, we are then at the global maximum. Then I did a "walking", a procedure where we touch one axis (so 2 knobs) after the other until we converge to a optimized value. Lastly, by adjusting more precisely the collimating lens on the optical axis, the power is maximized and we have our coupling efficiency.

After following the steps, I measured the input (output of the laser) and output power to calculate our efficiency. The whole procedure is done at low power to avoid damaging the fibre before it's correctly coupled, so I turned up the current to have the efficiency at higher power which can change slightly from weak power. I measured $P_{input} = 30.5mW$ and $P_{output} = 14.9mW$ which gives a coupling efficiency of approximately 50%. We can compare it to the setup in another one of the team's experiments which utilises the same laser diode, and they reached only 30% of coupling efficiency.

However, given the context, it does not seem worth it to lose half of the optical power for practicality when the optical chain could fit, with some adjustments, into a free-space setup. Nevertheless, this research process was not in vain because this result is still relevant to our setup, as it is the coupling efficiency that will be expected for the optical injection-lock.

4 Design of the optical chain

After having managed to create a laser beam round and stigmatic that can be used, the second part of my job consisted of designing the optical chain around it. Indeed, the laser needs to have certain characteristics: polarisation, size, before being sent into the vacuum chamber on the atoms. Plus,

the experiment is already very complex with a lot of optical tables and tools, so finding a space to place the chain in free space is complicated, and the space found will have constraints that need to be taken into consideration.

The space assigned for this project is situated in the immediate vicinity of the transverse cooling chamber. Two beams — one vertical and one horizontal — need to be directed into the vacuum chamber, originating from the same position they currently use. The only part of the current set-up that will be kept is the final telescope that enlarges the beam on the horizontal axis to maximise interaction time with the atoms.

Taking all this into consideration, the design I came up with is explained in Figure 9.

4.1 The components of the optical chain

Not accounting for the multiple mirrors whose only purpose is to redirect the light, the optical chain is composed of:

- The telescope mentioned above, made of a divergent and a convergent cylindrical lens, approximately 7 cm apart.
- An optical isolator, which is a component that only allows the transmission of light in one direction. It is used to prevent unwanted feedback into the laser diode, which could damage and disturb it. The feedback could interfere and compete with the master's light in the competition of mode, which would disrupt the injection-lock. The isolator is made of three parts: an input polariser, a Faraday rotator, and an output polariser, called an analyser. The polarisation of both polarisers can be changed manually. For example, it can be operated with the input one polarised vertically and the output one at 45°. When entering, the light will be polarised along the vertical axis, will rotate by 45° during the Faraday rotator and will exit without issue out of the 45° analyser. On the contrary, when the light comes back in the other direction, it will first be polarised at 45°. The polarisation will be rotated by 45° in the same direction, and the beam will reach the end of the medium polarised horizontally. It will not be able to exit the isolator as it will be stopped by the orthogonal analyser.
- Two $\lambda/2$ wave-plates framing the isolator.
- Two optical fibres placed in mounts with knobs. The first, surnamed "maître" in the schematic view, couples the laser diode beam with light coming from a master laser. This laser, composed of a diode whose cavity is closed by a mirror mounted on a piezoelectric, is controlled in frequency, and its light is injected into our laser diode. Before injection, the laser diode is hugely multimodal because of its wide spectral width. When light is injected, the competition of modes is shifted, and the whole gain goes toward the mode of the master laser. The laser will then emit light with the right frequency and small enough spectral width to excite the 461 nm transition of the atoms. The fibre used here is single-mode because it needs to transmit only the mode of the master laser. Given the coupling efficiency reached, some light can be

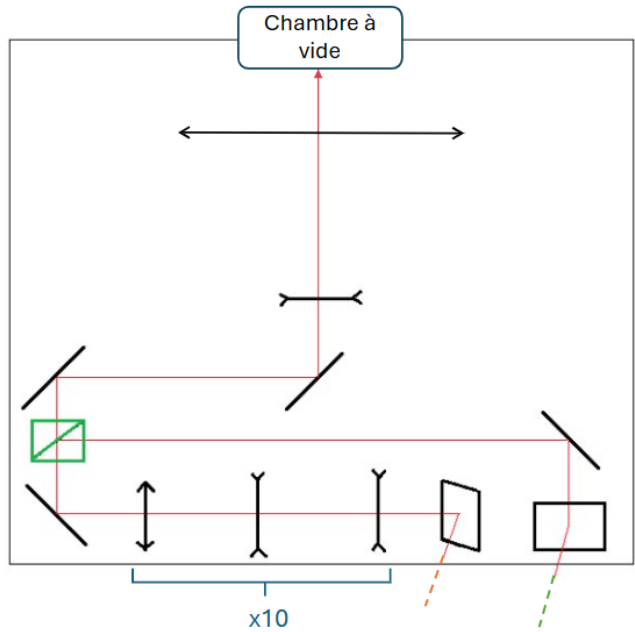
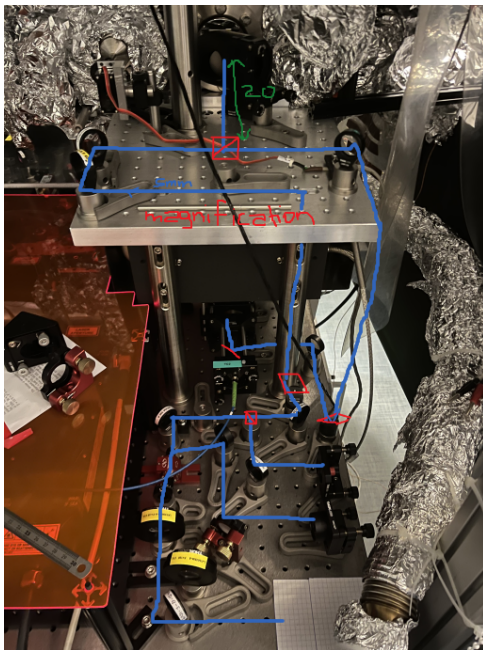
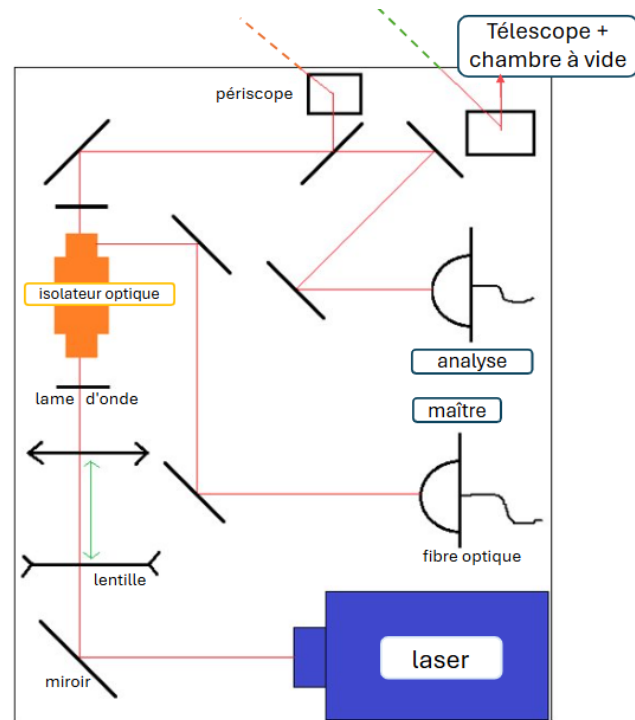
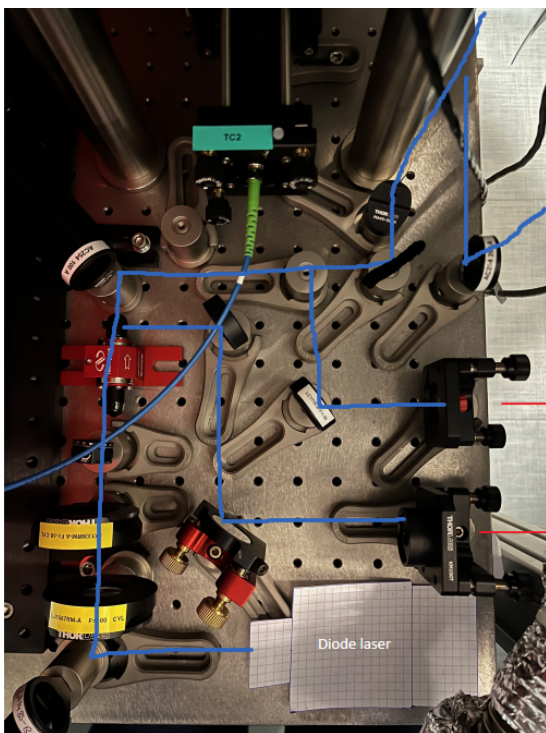


Figure 10: Representations of the top part (top) and bottom part (bottom) of the optical chain design. On the right are schematic views with the important elements that will be described later on and on the left side are pictures of a test done on the experiment to see if the design fits the constraints in place. There was a 20x30 cm area available in the bottom part and a square of 30x30 cm above.



lost in the fibre, but the injection only requires very little power, about 1 mW, so it's not an issue.

The second fibre allows us to transfer the beam to an analysis Fabry-Perot cavity. This cavity is formed of two reflective surfaces and the distance between them is configurable with a piezoelectric. For a given distance, only selective wavelengths will be emitted from the cavity. By scanning the distance, we are able to determine the wavelengths our laser emits, hence whether it's multimode or not. The cavity used for this laser is the same as for the other blue

injection-locked lasers and is located on the main optical table. For this analysis, not a lot of power is needed. That's why instead of placing a beam splitter that would divert some 10% of the power, we chose to use the weak transmission of one of the mirrors as a source for the fibre. The fibre used is multimodal, so all the light will be transmitted without loss and enough power will arrive at the cavity.

- Two periscopes to send light from the bottom panel to the top one, or inversely. There are composed of 2 mirrors mounted with knobs angled at 45° . A box will be placed all around the vertical beam and the mirrors to comply with laser safety rules.
- A system of magnification $\times 10$. To enter the telescope that was kept from the previous set-up, the beam needs to have a specific size of $w = 5\text{ mm}$. The dimension of our laser beam is, when entering this 3-lenses magnification system, $w \approx 500\mu\text{m}$. This necessitates the addition of a telescope multiplying by 10 the size of the beam. This can be done in a lot of ways; however given the constraints of space in the experiment, we need a system that takes less than 20 cm. This means lenses of short focal lengths. After consideration, we settled on a 3 lenses system with 2 divergent lenses (-20 mm and -50 mm) and a convergent one (100 mm). The design is shown in Figure 9.

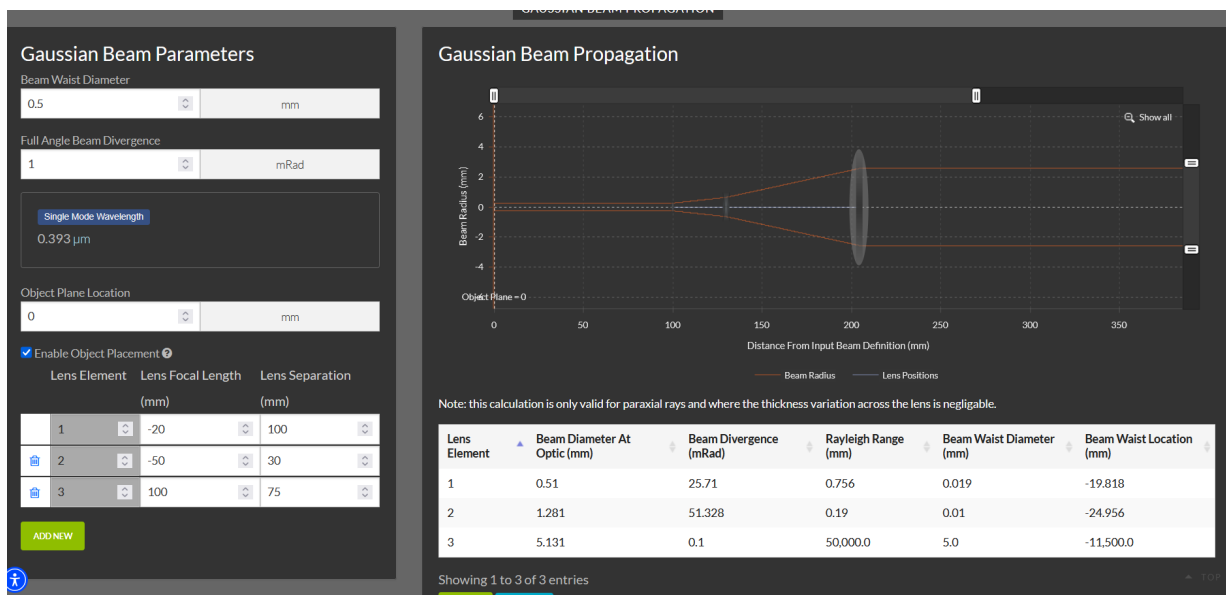


Figure 11: Capture of a test for the 3 lenses magnification system using the website lightmachinery.com (Gaussian beam propagation software). It shows the sequence of a -20 mm, -50 mm and 100 mm lenses and hints that it can create a beam of the wished waist in $30 + 75 = 105\text{ mm}$, ie 10.5 cm. The design would fit the constraints given by the space available in the experiment. The design will have to be tested to make sure the simulation is true and no aberrations are created.

Some concerns arose about the aberrations of such a system and the need to use achromatic doublet lenses instead of spherical singlets. After some testing on the optic design software Zemax, we concluded that there was a need for a doublet only for the $f = 100\text{ mm}$ lens. In that case, when adding in the simulation a perfect converging lens at the end of the system,

the whole beam focuses inside the Airy circle; therefore it is diffraction limited. The difference between this system and if another doublet was added was insignificant. Hence, the other lenses are simply spherical singlets.

- A polarising beam splitter 50:50. The light has to be split in half to create two beams for the two axes of the 2D optical molasses. The beam splitter is of a big dimension (edges = 20 mm) because it is situated after the magnification of the beam. The choice of this component landed on a polarising beam splitter because it gives the opportunity to control easily the percentage of each output by changing the polarisation of the light before the cube. It will be operated with a 45° polarisation, which gives equal power for both outputs, but if needed the polarisation can be slightly rotated towards one axis to optimise the number of atoms slowed.

The beam is finally magnified along the direction of the movement of the atoms by the last telescope. It enters the chamber through windows situated at the bottom and the side to interact with the atoms.

5 Conclusion

To conclude, we hope that in the near future the optical chain will be implemented in the experiment. As of now, it is still in construction. Such a setup requires precise and rigorous work that cannot be done in a hurry because of the consequences it could have in the entire sequence. Without the optical transverse cooling stage, the number of atoms in our final degenerate gas would consequently decrease, which would impact our ability to observe and study the desired physical phenomenon. In the event, the laser diode is not correctly calibrated, for example the frequency by the injection-lock, the size or the direction, the complete time sequence could be affected. Hence the job that was handed to me, a destructive work for the experimental setup, is of great importance. As soon as it is implemented, the goal will be to characterise the increase in gain obtained by the laser solution's replacement.

Nonetheless, by carrying on this previous researched on the laser diode : its working temperature, its characteristics, how to properly collimate it, how to change its shape and astigmatism, and its coupling efficiency, we possess all the tools to correctly build the optical chain.

In the short term, the plan is clear. The breadboard has been sized and fitted into the setup. First, components independent of the original setup—laser, optics, mirrors, and isolator—will be assembled. Next, the setup will be moved to the experimental room to connect optical fibres to the master laser and cavity. Then, the top part of the chain will be built and aligned with the bottom via the periscopes. Finally, both sections will be aligned with the original telescopes, requiring removal of the original laser fibres. With the chain ready, the next step will be to run the experiment and observe any increase or decrease in gain to perform a thorough calibration.

References

- [1] Domantas Burba et al. “Effective light-induced Hamiltonian for atoms with large nuclear spin”. In: *Phys. Rev. Research* 6 (2024). Also available as arXiv:2404.12429 [quant-ph], p. 033293. DOI: [10.1103/PhysRevResearch.6.033293](https://doi.org/10.1103/PhysRevResearch.6.033293). arXiv: [2404.12429 \[quant-ph\]](https://arxiv.org/abs/2404.12429). URL: <https://arxiv.org/abs/2404.12429>.
- [2] Husain Ahmed et al. “Coherent control over the high-dimensional space of the nuclear spin of alkaline-earth atoms”. In: *arXiv preprint* arXiv:2501.01731 (2025). Submitted 3 Jan 2025; revised 29 Apr 2025. DOI: [10.48550/arXiv.2501.01731](https://doi.org/10.48550/arXiv.2501.01731). arXiv: [2501.01731 \[quant-ph\]](https://arxiv.org/abs/2501.01731). URL: <https://arxiv.org/abs/2501.01731>.
- [3] Michael Foss-Feig et al. “Steady-state many-body entanglement of hot reactive fermions”. In: *Physical Review Letters* 109.23 (Dec. 4, 2012), p. 230501. ISSN: 0031-9007, 1079-7114. DOI: [10.1103/PhysRevLett.109.230501](https://doi.org/10.1103/PhysRevLett.109.230501). arXiv: [1207.4741 \[cond-mat\]](https://arxiv.org/abs/1207.4741). URL: <http://arxiv.org/abs/1207.4741>.
- [4] Pierre Bataille. “Réalisation de gaz quantiques de grand spin”. These de doctorat. Paris 13, Dec. 20, 2022. URL: <https://theses.fr/2022PA131098>.
- [5] Andréa Litvinov. “Manipulation des spins nucléaires du strontium 87 dans des gaz de Fermi dégénérés en symétrie SU(N)”. These de doctorat. Paris 13, Jan. 11, 2023. URL: <https://theses.fr/2023PA131062>.
- [6] Takashi Mukaiyama et al. “Recoil-Limited Laser Cooling of $^{87}\mathrm{Sr}$ Atoms near the Fermi Temperature”. In: *Physical Review Letters* 90.11 (Mar. 20, 2003). Publisher: American Physical Society, p. 113002. DOI: [10.1103/PhysRevLett.90.113002](https://doi.org/10.1103/PhysRevLett.90.113002). URL: <https://link.aps.org/doi/10.1103/PhysRevLett.90.113002>.
- [7] Félix Faisant. “Building a strontium quantum gas microscope”. These de doctorat. université Paris-Saclay, Dec. 4, 2024. URL: <https://theses.fr/2024UPASP147>.
- [8] Nichia Corporation. *Nichia Blue Laser Diode Part No. NDB4916 spec sheet*. Document PDF. Disponible en ligne : <https://led-ld.nichia.co.jp/api/data/spec/ld/NDB4916.pdf>.